Journal of Solid State Chemistry 182 (2009) 1040–1044

Contents lists available at ScienceDirect

Journal of Solid State Chemistry

journal homepage: www.elsevier.com/locate/jssc

Syntheses, structures and properties of a series of photochromic hybrids based on Keggin tungstophosphates

Li-Zhi Zhang [a,b], Wen Gu [b], Zhili Dong [a,*], Xin Liu [b,*], Bing Li [a,b], Mei-Ling Liu [b]

[a] School of Materials Science and Engineering, Nanyang Technological University, Singapore 639798, Singapore
[b] Department of Chemistry, Nankai University, Tianjin 300071, People's Republic of China

ARTICLE INFO

Article history:
Received 22 October 2008
Received in revised form
19 January 2009
Accepted 29 January 2009
Available online 6 February 2009

Keywords:
Polyoxometalates
Lanthanide
Photochromism
Magnetism
Luminescence

ABSTRACT

Three inorganic–organic hybrids based on Keggin tungstophosphates and lanthanides, $[Pr(NMP)_6(PW_{12}O_{40})]_n$ (**1**), $[Eu(NMP)_6(PW_{12}O_{40})]_n$ (**2**), and $[Er_2(NMP)_{12}(PW_{12}O_{40})][PW_{12}O_{40}]$ (**3**) (NMP = *N*-methyl-2-pyrrolidone), have been synthesized and characterized by elemental analysis, IR, UV–vis, and single-crystal X-ray diffraction. Compounds **1** and **2** exhibit 1D infinite zigzag chain structures, while compound **3** exhibits an ionic asymmetric structure due to lanthanide contraction. The three compounds are all photochromic. The magnetic susceptibility for **1** measured over the range 2–300 K shows that there is the dominant antiferromagnetic interaction in the compound. The results of luminescent properties show that compound **2** displays an interesting selectivity for Zn^{2+} ions.

1. Introduction

Polyoxometalates (POMs) are nano-sized metal-oxygen cluster species with a diverse compositional range and an enormous structural variety [1–3]. It is well-known that one of the most important properties of POMs is the capability to accept various numbers of electrons giving rise to mixed-valency colored species (heteropolyblues or heteropolybrowns) [4], which makes them suitable for photochromic and electrochromic materials [4–6]. Since the investigation of inorganic–organic hybrid materials became an expanding field, the preparation, microstructure, and photochromic process of POMs-based hybrid composites have been extensively investigated [7–11].

On the other hand, the rational design and synthesis of inorganic–organic hybrid architectures based on POMs and various metal coordination complexes are of considerable interest and of great challenge in current synthetic chemistry [12–23]. Comparing with large numbers of POMs-based hybrid materials structurally modified by transition metal elements [12–20], rare earth elements as the linkers have been paid less attention in assisting the self-assembly of POMs building blocks [21–23], although their compounds may possess potential applications in many fields. In most cases, it appears that oxygen atoms on the surface of POMs are rather reactive and are easily combined with the highly oxophilic rare earth ions to form precipitates instead of crystals. The introduction of protecting organic ligands may be one of the effective methods to inhibit precipitation by coordinating rare earth ions and decreasing their highly oxophilic properties [23].

Herein, by using the protecting ligand *N*-methyl-2-pyrrolidone (NMP), three lanthanide-linked photochromic hybrids based on $[PW_{12}O_{40}]^{3-}$ have been successfully synthesized. Their photochromic, magnetic, and luminescent properties have been investigated.

2. Experimental

2.1. Materials and methods

All reagents were purchased commercially and used without further purification. Elemental analyses (C, H, N) were conducted on a Perkin-Elmer 240C analyzer. Infrared spectra were obtained from a sample powder palletized with KBr on Nicolet AVATAR 360 FTIR spectrophotometer over the range of 4000–400 cm^{-1}. UV spectra were obtained on a Unican UV-500 spectrometer (distilled water as solvent) in the range of 190–1100 nm. Variable temperature susceptibility measurements were carried out in the temperature range 2–300 K at a magnetic field strength of 2 kG with a quantum design MPMS-7 SQUID magnetometer. Diamagnetic corrections were made with Pascal's constants for all

* Corresponding authors. Fax: +65 86 2350 5020.
E-mail addresses: zldong@ntu.edu.sg (Z. Dong), liuxin64@nankai.edu.cn (X. Liu).

0022-4596/$ - see front matter © 2009 Elsevier Inc. All rights reserved.
doi:10.1016/j.jssc.2009.01.037

the constituent atoms. The emission spectra in an aqueous solution were recorded on a Cary Eclipse luminescence spectrophotometer.

2.2. Synthesis of $[Pr(NMP)_6(PW_{12}O_{40})]_n$ (1)

Reaction of $H_3PW_{12}O_{40}\cdot nH_2O$ (1.3 g), $PrCl_3\cdot 6H_2O$ (0.142 g, 0.4 mmol) and *N*-methyl-2-pyrrolidone (0.5 mL) in an acetonitrile/water (2:1 v/v) mixed solution (10 mL) at 90 °C for 1 h followed by slow evaporation at room temperature in the dark resulted in colorless single crystals. Yield: 1.18 g (82%). Anal. Calcd (%): C 10.0, H 1.5, N 2.3; Found: C 10.4, H 1.6, N 2.1. IR (KBr, *v*): 3404 (s), 2936 (w), 1640(vs), 1516 (m), 1406 (w), 1308 (w), 1262 (w), 1256 (m), 1080 (vs), 985 (vs), 896 (vs), 813 (vs), 521(m) cm^{-1}. UV–vis (solid-state, λ_{max}): 250 nm.

2.3. Synthesis of $[Eu(NMP)_6(PW_{12}O_{40})]_n$ (2)

2 was prepared according to the procedure described for **1** but using $EuCl_3\cdot 6H_2O$ (0.147 g, 0.4 mmol) as the rare earth reagent. Yield: 1.12 g (77%). Anal. Calcd (%): C 9.9, H 1.5, N 2.3; Found: C 10.1, H 1.7, N 2.1. IR (KBr, *v*): 3404 (s), 2937 (w), 1639(vs), 1513 (m), 1406 (w), 1308 (w), 1260 (w), 1258 (m), 1080 (vs), 983 (vs), 895 (vs), 813 (vs), 521(m) cm^{-1}. UV–vis (solid-state, λ_{max}): 250 nm.

2.4. Synthesis of $[Er_2(NMP)_{12}(PW_{12}O_{40})][PW_{12}O_{40}]$ (3)

3 was prepared according to the procedure described for **1** but using $ErCl_3\cdot 6H_2O$ (0.153 g, 0.4 mmol) as the rare earth reagent. Yield: 1.15 g (79%). Anal. Calcd (%): C 9.9, H 1.5, N 2.3; Found: C 10.3, H 1.4, N 2.2. IR (KBr, *v*): 3402 (s), 2940 (w), 1634(vs), 1517 (m), 1403 (w), 1310 (w), 1260 (w), 1256 (m), 1078 (vs), 980 (vs), 895 (vs), 810 (vs), 516(m) cm^{-1}. UV–vis (solid-state, λ_{max}): 250 nm.

2.5. Crystal structure determination

Structural measurements of three complexes were performed on a computer controlled Bruker SMART 1000 CCD diffractometer equipped with graphite-monochromated Mo-$K\alpha$ radiation with radiation wavelength of 0.71073 Å by using the ω-scan technique. Lorentz polarization and absorption corrections were applied. The structures were solved by direct methods using the program SHELX 97 and subsequent Fourier difference techniques, and refined anisotropically by full-matrix least-squares on F^2 using SHELXL 97. The summary of crystallographic data is given in Table 1.

Crystallographic data (excluding structure factors) for the structural analysis have been deposited with the Cambridge crystallographic data centre, CCDC nos. 294255, 611820, and 611432 for structures of the three compounds. Copies of this information may be obtained free of charge from the director, CCDC, 12 Union Road, Cambridge, CB2 1EZ, UK (fax: +44 1223 336 033; e-mail: deposit@ccdc.cam.ac.uk or www: http://www.ccdc.cam.ac.uk).

3. Results and discussion

X-ray analyses reveal that **1** and **2** are isomorphous. The two compounds, crystallized as $[Ln(NMP)_6(PW_{12}O_{40})]_n$ (Ln = Pr (**1**), Eu (**2**)), consist of 1D infinite zigzag chains built from alternate polyanions and $[Ln(NMP)_6]^{3+}$ subunits, displaying a {(anion) *M*-donor}$_n$ ($M = Ln$; anion = $PW_{12}O_{40}^{3-}$; donor = NMP) type of structure (Fig. 1). The adjacent $Ln\cdots Ln$ distances are 15.540 Å for **1** and 15.442 Å for **2**, respectively. The coordination polyhedron of Ln^{III} can be represented as a distorted, bicapped trigonal prism (Fig. 2). In **1**, the Pr–O bond lengths are within the range from 2.326 to 2.579 Å (mean value 2.414 Å). The torsion angle between the top plane and the bottom plane is 7.52°. In **2**, the Eu–O bond lengths are within the range from 2.256 to 2.503 Å (mean value 2.355 Å). The torsion angle between the top plane and the bottom plane is 7.66°.

Interestingly, different from **1** and **2**, compound **3** exhibits an ionic, asymmetric structure probably because of the lanthanide contraction. Compound **3** consists of the $[PW_{12}O_{40}]^{3-}$ anion and the $[Er_2(NMP)_{12}(PW_{12}O_{40})]^{3+}$ cation in which either of Er^{III} ions is coordinated with 6 NMP molecules and connected by $[PW_{12}O_{40}]^{3-}$ (Fig. 3). The adjacent Er···Er distance is 15.353 Å. The coordination polyhedron of Er^{III} can be represented as a highly distorted, single-capped trigonal prism (Fig. 4). The Er–O bond lengths are within

Table 1
Crystal data and structure refinement for compounds **1**, **2** and **3**.

Compound	1	2	3
Empirical formula	$C_{30}H_{54}N_6O_{46}PPrW_{12}$	$C_{30}H_{54}N_6O_{50}PEuW_{12}$	$C_{60}H_{108}Er_2N_{12}O_{92}P_2W_{24}$
M_r	3612.87	3623.92	7278.44
T (K)	294(2)	294(2)	294(2)
λ (Å)	0.71073	0.71073	0.71073
Crystal system	Monoclinic	Monoclinic	Triclinic
Space group	$C2/c$	$C2/c$	$P\bar{1}$
a (Å)	22.021(3)	21.979(3)	12.1107(18)
b (Å)	12.9042(19)	12.7848(17)	13.592(2)
c (Å)	24.288(4)	24.310(3)	22.219(3)
α (deg)	90	90	80.242(2)
β (deg)	106.823(2)	107.303(2)	85.464(2)
γ (deg)	90	90	67.550(3)
V (Å^3)	6606.4(16)	6522.2(15)	3330.9(9)
Z	4	4	1
D_c (g/cm^3)	3.632	3.691	3.629
F (000)	6424	6440	3230
$2\theta_{max}$ (deg)	50.02	50.02	50.04
R_{int}	0.0648	0.0652	0.0399
GOF on F^2	1.011	1.067	1.072
$R1$	0.0429	0.0602	0.0645
$wR2$	0.1095	0.1620	0.1636

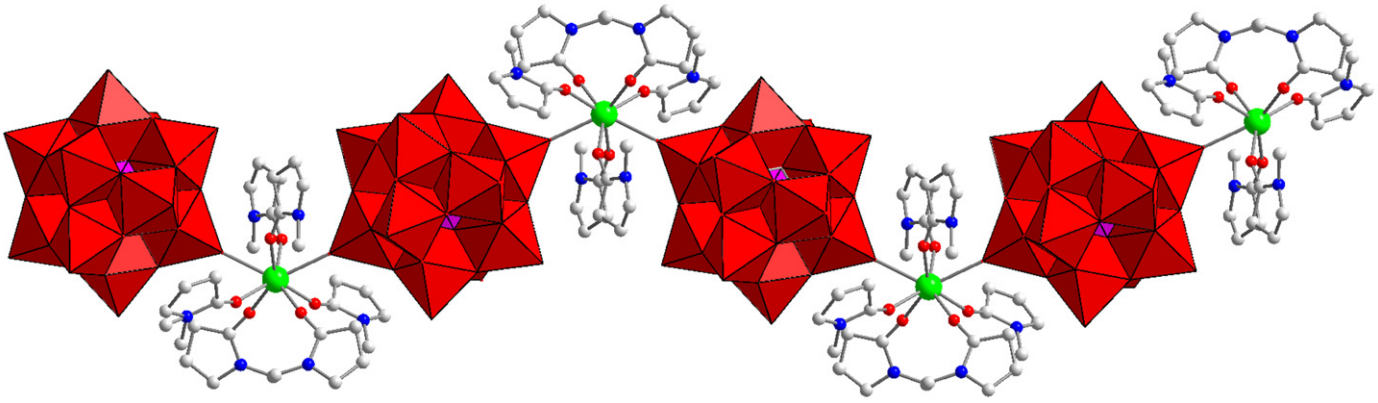

Fig. 1. Ball and stick and polyhedral representations of the 1D infinite zigzag chain structure of compound **1** (compound **2** is isomorphous to **1**). The color code is as follows: Pr (green), O (red), N (blue), C (gray), WO_6 (red), PO_4 (purple). (For interpretation of the references to color in this figure legend , the reader is referred to the web version of this article.)

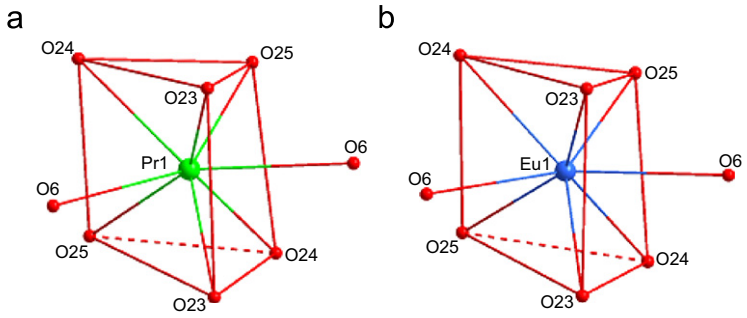

Fig. 2. (a) Coordination polyhedron around Pr^{III} in **1**; (b) coordination polyhedron around Eu^{III} in **2**. Bond lengths (Å): (a) Pr(1)–O(6), 2.579(10); Pr(1)–O(23), 2.364(12); Pr(1)–O(24), 2.387(13); Pr(1)–O(25), 2.326(13); (b) Eu(1)–O(6), 2.503(3); Eu(1)–O(23), 2.305(2); Eu(1)–O(24); 2.357(2); Eu(1)–O(25), 2.256(2).

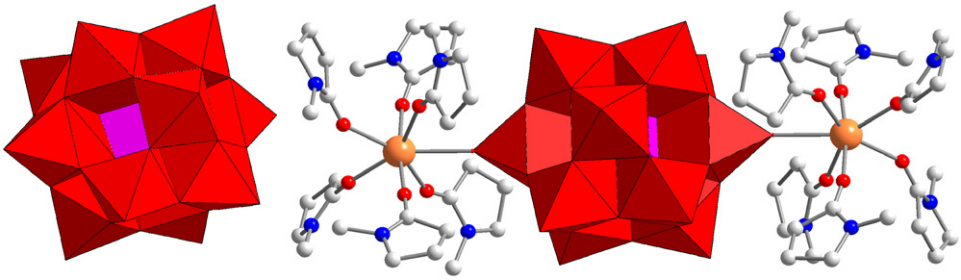

Fig. 3. Ball and stick and polyhedral representations of the ionic asymmetric structure of compound **3**. The color code is as follows: Er (orange), O (red), N (blue), C (gray), WO_6 (red), PO_4 (purple). (For interpretation of the references to color in this figure legend, the reader is referred to the web version of this article.)

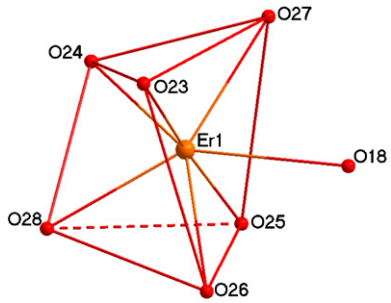

Fig. 4. Coordination polyhedron around Er^{III} in **3**. Bond lengths (Å): Er(1)–O(18), 2.416(15); Er(1)–O(23), 2.18(2); Er(1)–O(24), 2.234(19); Er(1)–O(25), 2.192(19); Er(1)–O(26), 2.343(18); Er(1)–O(27), 2.254(18); Er(1)–O(28), 2.236(18).

the range from 2.18 to 2.416 Å (mean value 2.265 Å). The torsion angle between the top plane and the bottom plane is 28.42°.

When exposed to sunlight, colorless crystals of **1–3** can turn deep blue gradually. This observation should be attributed to the electron transfer between electron donors of organic molecules and electron acceptors of polyoxometalate anions. The final result is that W^{VI} atoms of the polyanions are reduced and mixed-valence compounds are formed, leading to the observed photochromism [4]. As shown in Fig. 5, after irradiation with sunlight, the absorption band at 700 nm in visible region appeared due to metal-to-metal extra intervalence charge transfer (IVCT) ($W^{5+} \rightarrow W^{6+}$) [1]. The photochromic mechanism of **1–3** should be similar to that well-reported in charger-transfer alkylammonium-polyoxometalates [4]. The reasonable mechanism should involve

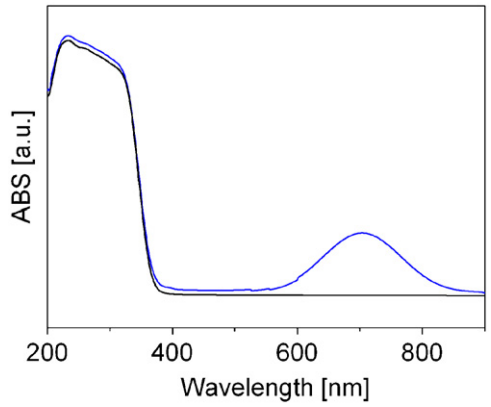

Fig. 5. The solid-state UV–vis spectra for compound **2** before (black curve) and after (blue curve) irradiation with sunlight. (For interpretation of the references to color in this figure legend, the reader is referred to the web version of this article.)

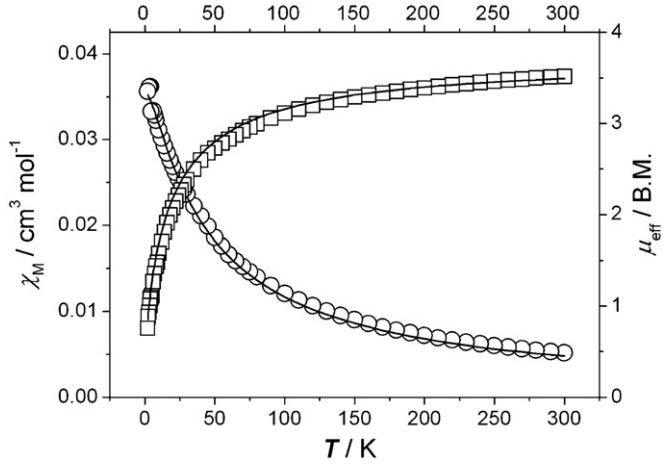

Fig. 6. χ_M (O) vs T and μ_{eff} (□) vs T plots for compound **1**. The solid lines represent the theoretical values based on the equations.

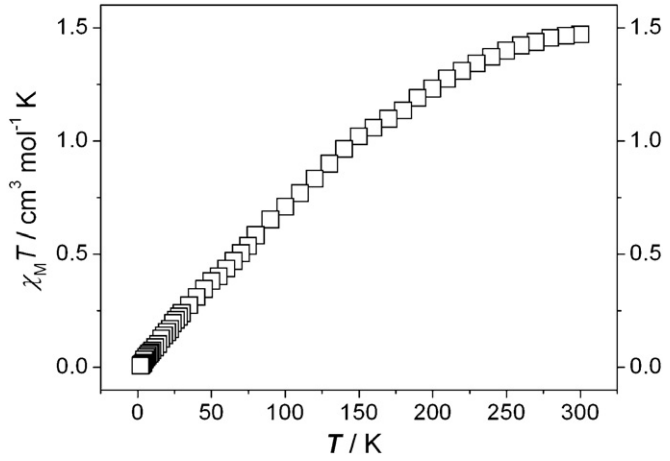

Fig. 7. $\chi_M T$ (□) vs T plots for compound **2**.

the absorption of photons by the Keggin structure, resulting in the generation of an electron–hole pair which directly oxidizes NMP into NMP^+.

Variable-temperature (2–300 K) magnetic susceptibility data at a magnetic field strength of 2 kG were collected for compound **1** (Fig. 6). The μ_{eff} value at room temperature was 3.52 B.M., which is

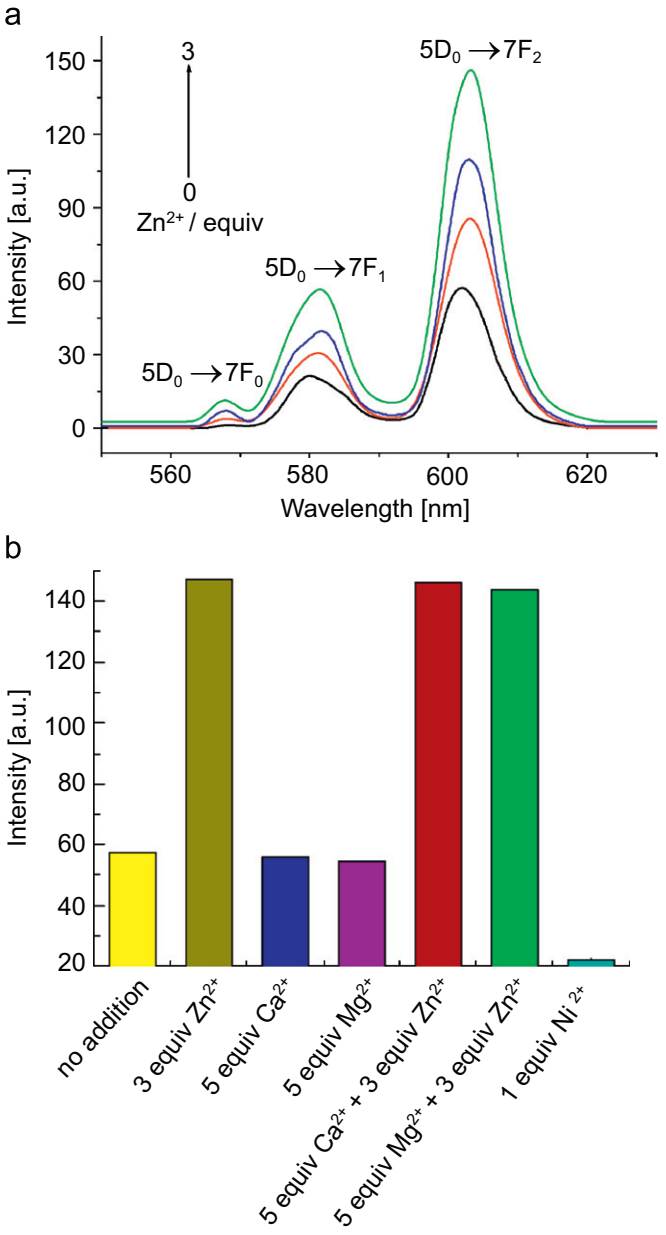

Fig. 8. (a) Emission spectra of compound **2** in an aqueous solution (5×10^{-3} M) at room temperature (excited at 289 nm) upon addition of ~0–3 equiv of Zn^{2+} ions, respectively: black, no addition; red, 1 equiv; blue, 2 equiv; green, 3 equiv; (b) Luminescent intensity of the compound at 603 nm in aqueous solution at room temperature upon addition of Zn^{2+}, Ca^{2+}, Mg^{2+} or Ni^{2+} ions (excited at 289 nm). Cations were added as $ZnCl_2$, $CaCl_2$, $MgCl_2$ or $NiCl_2$. (For interpretation of the references to color in this figure legend, the reader is referred to the web version of this article.)

slightly lower than that expected, 3.58 B.M., per insulated Pr(III) ion in the $^3H_4$ ground state ($g = 4/5$). As far as the existence of a strong spin–orbit coupling for *Ln* atoms is concerned, the magnetic data were analyzed by the following approximate treatment equations previously derived by McPherson et al. [24].

$$\chi_{Pr} = \frac{Ng^2\beta^2}{kT}\frac{2\exp(-\Delta/kT) + 8\exp(-4\Delta/kT) + 18\exp(-9\Delta/kT) + 32\exp(-16\Delta/kT)}{1 + 2\exp(-\Delta/kT) + 2\exp(-4\Delta/kT) + 2\exp(-9\Delta/kT) + 2\exp(-16\Delta/kT)}$$

$$\chi_{total} = \chi_{Pr}/[1 - \chi_{Pr}(zJ'/Ng^2\beta^2)]$$

In expressions, Δ is the zero-field-splitting parameter. zJ' is the intermolecular magnetic coupling parameter. Best fitting for the

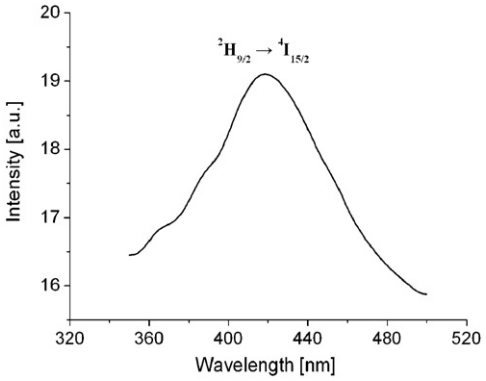

Fig. 9. Emission spectra of **3** (5×10^{-3} M) at room temperature (excited at 320 nm) in an aqueous solution.

experimental data leads to $\Delta = -0.910\,cm^{-1}$, $zJ' = -4.719\,cm^{-1}$, $g = 0.806$, and $R = \sum(\chi_{obsd}-\chi_{cacld})^2/\sum(\chi_{obsd})^2 = 1.73 \times 10^{-3}$.

Variable-temperature (2–300 K) magnetic susceptibility data at a magnetic field strength of 2 kG were collected for compound **2** (Fig. 7). At room temperature, the observed $\chi_M T$ value of **2** is ca. 1.47 $cm^3\,mol^{-1}\,K$, slightly less than the value 1.5 for a Eu(III) ion calculated by Van Vleck equation allowing for population of the excited state with higher values of J at 293 K [25]. As the temperature is lowered, $\chi_M T$ decreases continuously as a result of the depopulation of the levels with nonzero J values. At the lowest temperature, $\chi_M T$ is close to zero, indicating a $J = 0$ ground state of the Eu(III) ion ($^7F_0$).

The emission spectrum of **2** (Fig. 8a) at room temperature in an aqueous solution excited at 289 nm exhibited the characteristic transition of the Eu^{3+} ion: $^5D_0 \rightarrow {}^7F_J$ ($J = 0, 1, 2$) [26]. Interestingly, upon addition of 1–3 equiv of Zn^{2+} gradually, the emission intensity of **1** obviously increased. The highest peak at 603 nm is closely thrice as intense as the corresponding band in the solution without Zn^{2+}. However, when the same experiments were performed for the introduction of Ca^{2+} and Mg^{2+} into the system, even the presence of five equiv of Ca^{2+} or Mg^{2+} in aqueous solution of **1** had no effect on the luminescent intensities either (Fig. 8b). While adding 1–3 equiv of transition metal ions such as Ni^{2+}, Co^{2+}, Mn^{2+}, and Fe^{2+} to the solution of the compound, the luminescent intensities decreased or quenched (Fig. 8b). The above results imply that compound **2** could monitor or recognize Zn^{2+} to some extent and be considered as luminescent probes.

The emission spectra of **3** (Fig. 9) at room temperature in aqueous solution excited at 320 nm exhibited an intense band at about 425 nm, which was assigned to the emission of $^2H_{9/2} \rightarrow {}^4I_{15/2}$ [27]. Upon addition of Zn^{2+}, Ca^{2+}, or Mg^{2+} to perform the same experiments to compound **2**, however, the emission intensity of **3** had no effect, only decreased or quenched when transition ions were added. The results indicate that the Zn^{II}-selective sensor properties in this system might be connected with the central lanthanide ions.

4. Conclusion

In summary, a series of inorganic–organic hybrids built on Keggin tungstophosphates have been prepared. Compounds **1** and **2** exhibit 1D infinite zigzag chain structures, while compound **3** exhibits an ionic asymmetric structure due to lanthanide contraction. Their photochromic, magnetic, and luminescent properties have been well studied. Especially, compound **2** displays an interesting luminescent selectivity for Zn^{2+} ions.

Acknowledgments

We are thankful for financial support from the National Natural Science Foundation of China (Grants 20771062, 20371027, and 20071020), the Tianjin Science Foundation (Grants 08JCZDJC21100 and 033609211), and the NTU Research Scholarship.

Appendix A. Supplementary Material

Supplementary data associated with this article can be found in the online version at doi:10.1016/j.jssc.2009.01.037.

References

[1] M.T. Pope, Heteropoly and Isopoly Oxometalates, Springer, Berlin, 1983.
[2] M.T. Pope, A. Müller, Angew. Chem. Int. Ed. 30 (1991) 34.
[3] C. Hill (Ed.), Special Issue on Polyoxometalates, Chem. Rev. 98 (1998) (special issue).
[4] T. Yamase, Chem. Rev. 98 (1998) 307.
[5] I. Moriguchi, J.H. Fendler, Chem. Mater. 10 (1998) 2205.
[6] S.Q. Liu, D.G. Kurth, H. Möhwald, D. Volkmer, Adv. Mater. 14 (2002) 225.
[7] C.L. Hill, D.A. Bouchard, M. Kadkhodayan, M. Williamson, J.A. Schmidt, E.F. Hilinski, J. Am. Chem. Soc. 110 (1988) 5471.
[8] G.R. Pedro, L.C. Morica, Adv. Mater. 9 (1997) 144.
[9] P. Maguerès, S.M. Hubig, S.V. Lindeman, P. Veya, J.K. Kochi, J. Am. Chem. Soc. 122 (2000) 10073.
[10] G. Zhang, W. Yang, J. Yao, Adv. Funct. Mater. 15 (2005) 1255.
[11] S. Liu, H. Möhwald, D. Volkmer, D.G. Kurth, Langmuir 22 (2006) 1949.
[12] J. Lu, E. Shen, M. Yuan, Y. Li, E. Wang, C. Hu, L. Xu, J. Peng, Inorg. Chem. 42 (2003) 6956.
[13] V. Shivaiah, M. Nagaraju, S.K. Das, Inorg. Chem. 42 (2003) 6604.
[14] H. An, Y. Li, E. Wang, D. Xiao, C. Sun, L. Xu, Inorg. Chem. 44 (2005) 6062.
[15] C.-M. Liu, D.-Q. Zhang, M. Xiong, D.-B. Zhu, Chem. Commun. (2002) 1416.
[16] J. Lu, Y. Xu, N.K. Goh, L.S. Chia, Chem. Commun. (1998) 2733.
[17] P.-Q. Zheng, Y.-P. Ren, L.-S. Long, R.-B. Huang, L.-S. Zheng, Inorg. Chem. 44 (2005) 1190.
[18] M.I. Khan, E. Yohannes, D. Powell, Chem. Commun. (1999) 23.
[19] M.I. Khan, E. Yohannes, R.J. Doedens, Angew. Chem. Int. Ed. 38 (1999) 1292.
[20] S.-T. Zheng, J. Zhang, G.-Y. Yang, Inorg. Chem. 44 (2005) 2426.
[21] A. Dolbecq, P. Mialane, L. Lisnard, J. Marrot, F. Sécheresse, Chem. Eur. J. 9 (2003) 2914.
[22] J. Lu, E. Shen, Y. Li, D. Xiao, E. Wang, L. Xu, Cryst. Growth Des. 5 (2005) 65.
[23] H. Zhang, L. Duan, Y. Lan, E. Wang, C. Hu, Inorg. Chem. 42 (2003) 8053.
[24] I.A. Kahwa, J. Selbin, C.J. Oconnor, J.W. Foise, G.L. McPherson, Inorg. Chim. Acta 148 (1988) 265.
[25] Z. He, E.-Q. Gao, Z.-M. Wang, C.-H. Yan, M. Kurmoo, Inorg. Chem. 44 (2005) 862.
[26] G. Vicentini, L.B. Zinner, J. Zukerman-Schpector, K. Zinner, Coord. Chem. Rev. 196 (2000) 353.
[27] A. Patra, C.S. Friend, R. Kapoor, P.N. Prasad, J. Phys. Chem. B. 106 (2002) 1909.